International Journal of Applied Earth Observation and Geoinformation 52 (2016) 115–125

Contents lists available at ScienceDirect

International Journal of Applied Earth Observation and Geoinformation

journal homepage: www.elsevier.com/locate/jag

Optimization of spectral indices and long-term separability analysis for classification of cereal crops using multi-spectral RapidEye imagery

Henning Gerstmann[a,*], Markus Möller[a,b], Cornelia Gläßer[a]

[a] Martin Luther University Halle-Wittenberg, Institute for Geosciences and Geography, Department for Remote Sensing and Cartography, Von-Seckendorff-Platz 4, 06120 Halle (Saale), Germany
[b] Martin Luther University Halle-Wittenberg, Institute of Agriculture and Nutrition Science, Department of Farm Management, Karl-Freiherr-von-Fritsch-Str. 4, 06120 Halle (Saale), Germany

ARTICLE INFO

Article history:
Received 1 March 2016
Received in revised form 1 June 2016
Accepted 2 June 2016

Keywords:
Vegetation index
Spectral separability
Crop classification
Time series
RapidEye

ABSTRACT

Crop monitoring using remotely sensed image data provides valuable input for a large variety of applications in environmental and agricultural research. However, method development for discrimination between spectrally highly similar crop species remains a challenge in remote sensing. Calculation of vegetation indices is a frequently applied option to amplify the most distinctive parts of a spectrum. Since no vegetation index exist, that is universally best-performing, a method is presented that finds an index that is optimized for the classification of a specific satellite data set to separate two cereal crop types. The η^2 (*eta-squared*) measure of association – presented as novel spectral separability indicator – was used for the evaluation of the numerous tested indices. The approach is first applied on a RapidEye satellite image for the separation of winter wheat and winter barley in a Central German test site. The determined optimized index allows a more accurate classification (97%) than several well-established vegetation indices like *NDVI* and *EVI* (<87%). Furthermore, the approach was applied on a RapidEye multi-spectral image time series covering the years 2010–2014. The optimized index for the spectral separation of winter barley and winter wheat for each acquisition date was calculated and its ability to distinct the two classes was assessed. The results indicate that the calculated optimized indices perform better than the standard indices for most seasonal parts of the time series. The red edge spectral region proved to be of high significance for crop classification. Additionally, a time frame of best spectral separability of wheat and barley could be detected in early to mid-summer.

1. Introduction

Crop classification using remote sensing data is becoming increasingly important for land use/land cover analysis, for agricultural and environmental research and management as well as for administrative purposes on regional scale levels. However, classification of crops, especially cereal species like wheat and barley, is often restricted due to high spectral similarity of the cropland classes (Guerschman et al., 2003) and sensor-specific limitations regarding temporal, spectral and geometric resolution of the currently available satellite sensors. The first limitation can be addressed using multi-temporal classification approaches which usually lead to significantly higher accuracies (e.g., Murakami et al., 2001; Van Niel and McVicar, 2004; Guerschman et al., 2003; Prishchepov et al., 2012; Löw et al., 2015) while the latter limitation will decline as consequence of the rapid increase of available imagery of both high temporal and geometric resolution acquired by modern sensors like Sentinel-2 or RapidEye (Simmons et al., 2016).

High spectral similarity of classes can also be addressed by the selection of the most significant parts of the reflectance spectrum which is usually performed by computation of vegetation indices. These indices are combinations of mostly two or three spectral channels that amplify spectral information of high significance for a distinction of different land cover classes. The most popular indices are the *Normalized Difference Vegetation Index* (*NDVI*, Rouse et al., 1974), the *Soil-adjusted Vegetation Index* (*SAVI*, Huete, 1988) and the *Enhanced Vegetation Index* (*EVI*, Liu and Huete, 1995). The majority

* Corresponding author. Tel.: +49 34528303.
E-mail addresses: henning.gerstmann@geo.uni-halle.de (H. Gerstmann), markus.moeller@landw.uni-halle.de (M. Möller), cornelia.glaesser@geo.uni-halle.de (C. Gläßer).

http://dx.doi.org/10.1016/j.jag.2016.06.001
0303-2434/

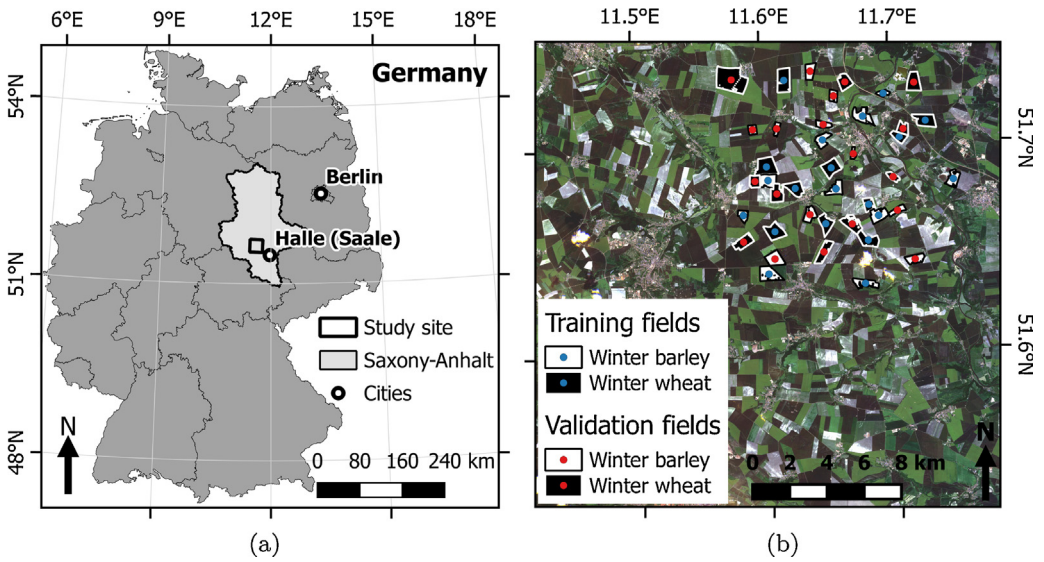

Fig. 1. Location of the study site (a) and training and validation parcels for the season 2014 laid over a RapidEye image acquired on 4th June 2014 (b). RGB band combination 3-2-1. Spatial reference: EPSG 32632 (Spatialreference, 2016).

of vegetation indices focuses on the spectral region between red and near infrared where reflectance of vital plants is characterized by a strong increase. A few sensors (e.g., RapidEye, Sentinel-2) have additional red edge channels between red and near infrared parts of the spectrum, and several studies demonstrated the potential of red edge reflectance information to increase land cover classification accuracies (Ramoelo et al., 2012; Schuster et al., 2012; Eitel et al., 2011).

Numerous vegetation indices have been developed over the past 40 years (see e.g., Dorigo et al., 2007; Bannari et al., 1995) for mapping of different vegetation parameters. However, Rivera et al. (2014) stated, that a specific index is not necessarily the best performing index to address the studied parameter for which the index is reported to be sensitive. Furthermore, vegetation index profiles computed from index values of different acquisition dates reveal differences in the separability of certain vegetation classes over time. To select the most sensitive index for a specific application and a specific time, Le Maire et al. (2008) proposed a brute-force approach for the selection of the optimal vegetation index to retrieve biophysical parameters of forests. Based on this idea, Rivera et al. (2014) developed a tool (*Automated Radiative Transfer Models Operator – ARTMO*) that calculates a huge number of possible vegetation indices and band combinations within an iterative loop and evaluates the performance of each tested index in regression-based estimation of a biophysical parameter. However, regression methods require the dependent variable to be at least interval-scaled, which is not given for categorical scaled land cover classes.

In this study, we first show how optimized indices can be calculated in an automatic manner for a mono-temporal data set selected out of a time series by phenological analysis. In this context, we introduce the measure of association η^2 (*eta-squared*) as novel non-parametric indicator for spectral separability. Second, we demonstrate how separability profiles can be computed using the full time series to describe separability variations within one year and different years applying spectral similarity measures. Consequently, optimal times frames for classification can finally be determined.

The approach is applied on a time series of RapidEye satellite data with high temporal resolution for the separation of winter wheat and winter barley in a Central German test site.

2. Study site and data

2.1. Site description

The study site is located in Central Germany (Fig. 1a), approximately 30 km north of the city of Halle (Saale). The site is characterized by intensive agricultural land use due to its highly fertile chernozemic soils and relatively warm climatic conditions. Cultivation data on parcel scale were obtained from the Ministry of Agriculture and Environment of Saxony-Anhalt and used as ground truth information. The most frequently grown crop types within the study site are winter wheat (≈45–48% of the total cropped area between 2010 and 2014), winter oilseed rape (17–20%) and winter barley (≈8–9%). Since oilseed rape can easily be separated from wheat and barley during flowering, the two cereals winter wheat and winter barley have been selected as target crops for this study due to their close genetic relationship and similar spectral behavior.

2.2. Satellite data

RapidEye data was obtained from the *RapidEye Science Archive*[1] which is funded by German Aerospace Center (*Deutsches Zentrum für Luft- und Raumfahrt*; DLR) and gains restricted access to RapidEye imagery. RapidEye is a commercial multi-spectral sensor constellation which consists of five identically constructed satellites (Tyc et al., 2005). The constellation provides imagery with high repetition rate, a spatial resolution of 6.5 m × 6.5 m, and five multi-spectral bands which cover the blue (R_B: 440–510 nm), green (R_G: 520–590 nm), red (R_R: 630–685 nm) and near infrared spectral ranges (R_{NIR}: 760–850 nm). In addition, a red edge band (R_{RE}: 690–730 nm) is available which is assumed to be sensitive to the abrupt reflectance rise caused by vegetation's chlorophyll status (Schuster et al., 2012).

The time series used in this study covers five years and consists of 43 images (Fig. 2). While the RapidEye constellation technically allows a repetition rate of less then a week, far less appropriate images are available mostly due to cloud cover and order prioritization. The temporal coverage of the time series is inconsistent

[1] *RESA* www.resa.blackbridge.com, project ID: 653.

Table 1
Well-established indices and required parameter configuration.

I^s	B_1	B_2	B_3	c_1	c_2	L	G	Reference
NDVI	R_{NIR}	R_R	–	1	1	–	1	Rouse et al. (1974)
GNDVI	R_{NIR}	R_G	–	1	1	–	1	Gitelson et al. (1996)
EVI	R_{NIR}	R_R	R_B	6	7.5	1	2.5	Huete et al. (1999)
EVI2	R_{NIR}	R_R	–	2.4	0	1	2.5	Jiang et al. (2008)
SAVI	R_{NIR}	R_R	–	1	1	0.5	1.5	Huete (1988)
EVI^{RE}	R_{NIR}	R_R	R_B	6	7.5	1	2.5	–
$NDVI^{RE}$	R_{NIR}	R_{RE}	–	1	1	–	1	Barnes et al. (2000)

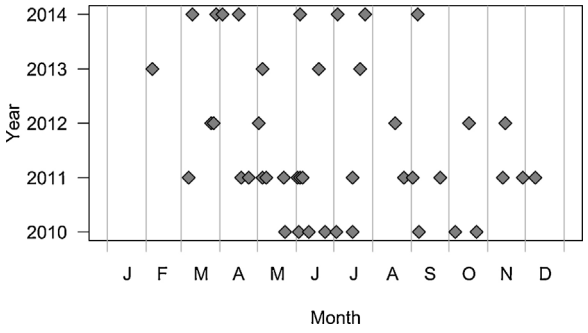

Fig. 2. Available RapidEye images.

throughout the years, varying from four images in 2013 to 16 scenes in 2011. No images from late spring and summer were available for 2012, while in 2010 and 2013 no early and mid-spring scenes could be used. All data sets were obtained at preprocessing level 3A, which means that radiometric, sensor, geometric corrections and geo-referencing were applied by the data provider. Each image covers 25 km × 25 km with orthorectified pixel size of 5 m × 5 m.

2.3. Selection of training fields

Twenty fields per year for each of the crop types winter wheat and winter barley were selected, 10 for training and validation, respectively (Fig. 1b). They were chosen under the premises that they have no *NoData* parts during the vegetation periods, no clouds and no snow coverage.

2.4. Phenological data

To characterize the typical growth cycle, phenological observations were analyzed. The date of entry of selected phenological phases for a variety of tree and agricultural species including winter wheat and winter barley are continuously recorded following standardized criteria by volunteer observers, managed by the German Weather Service (Deutscher Wetterdienst, 2015). The observations can be accessed via FTP[2].

3. Methods

3.1. Index permutation

The computation for the most vegetation indices is based on a normalized-difference rationale with only different spectral bands included. Equation (1) represents the structure of the formula used for the index permutation which is equivalent to the formula used for the calculation of the *EVI* (Huete et al., 1999). Within Eq. (1), B_1, B_2 and B_3 can be any of the spectral bands; i represents all possible combinations of B_1, B_2 and B_3 and the empirical constants G, c_1, c_2 and L.

$$I_i^{perm} = G \times \frac{B_1 - B_2}{B_1 + c_1 \times B_2 - c_2 \times B_3 + L} \quad c_1, c_2, L, G \in \mathbb{R} \tag{1}$$

A set of well-established indices (I^s) was calculated for comparison. I^s contains vegetation indices and red-edge-modified variants which are an element of I_i^{perm} (see Table 1) as well as others which are not included. The latter are the *Wide Dynamic Range Vegetation Index* (*WDRVI*, Gitelson, 2004), which is computed similarly to *NDVI* but with a scaling of the near infrared reflectance by 0.15, the *Green Chlorophyll Index* (*CIgreen*, Wu et al., 2012), which is calculated by subtraction of 1 of the NIR/blue ratio, and the *simple NIR/Red edge ratio* (*SRR*; Ramoelo et al., 2012). Since spectrally very similar crop types are expected to show significant but narrow differences in the red edge region, the red edge variants of the established *NDVI* and *EVI* are mainly addressed within this study. Furthermore, indices calculated from the red and near infrared reflectance tend to show higher saturation effects than indices were the red band is replaced by the red edge reflectance information (e.g., Eitel et al., 2011).

3.2. Spectral similarity assessment

The indices calculated by permutation of Eq. (1) can be understood as interval-scaled variable, while class information is of nominal scale. Thus correlation coefficients like Pearson's r and Spearman's ρ cannot be used for the assessment of the index performance. However, the effect-size measure η^2 can be understood as correlation coefficient assessing the influence of class membership and index value. The metric is calculated by $\eta^2 = SS_B/SS_T$, where SS_B is the sum of the squared differences of each index value to the class-specific mean, and SS_T is the sum of the squared differences of each index value to the overall mean. The values range from 0 to 1, where values higher than 0.26 indicate a strong dependency of the predicted variable on the predictor (*Cohen's rule of thumb*, Cohen, 1988). In the classification case, class membership is the predictor variable on which the vegetation index value depends on.

The capability of η^2 to quantify spectral similarity is compared to the often applied *Kolmogorov–Smirnov distance* (d^{KS}). These two metrics were selected to address the fact that vegetation indices and remote sensing data in general are not necessarily normally distributed (Swain and Davis, 1978). Both metrics can be used to compare distributions without requiring statistical preconditions like normal distribution. Other often applied distances measures like *Jeffries–Matusita distance* (Vaiphasa et al., 2005) and *divergence* (Swain and Davis, 1978) are inappropriate since they are based on the maximum-likelihood decision rule and thus require normally distributed class samples (Richards, 2012).

The *Kolmogorov–Smirnov distance* d^{KS} was proposed by Kolmogorov (1933) and is defined as the maximal difference between the empirical cumulative distribution functions (*ECDF*) of two samples (Massey, 1951). Values of $d^{KS} \simeq 1$ indicate high separability while identical spectra are characterized by d^{KS} close to 0. This measure has been frequently applied in remote sensing for feature selection, class separability assessment and multi-temporal change

[2] ftp.dwd.de/pub/CDC/observations_germany/phenology/.

Table 2
Domains of parameters which are permuted for index calculation.

B_1, B_2, B_3	c_1, c_2	L	G
$[R_B, R_G, R_R, R_{RE}, R_{NIR}]$	[−1, 0, 1, 2.4, 6, 7.5]	[−1, −0.5, 0, 0.5, 1]	[1, 1.5, 2.5]

Table 3
Mean observed day of year (*DOY*) for selected phenological phases within the study site and range between earliest and latest observation between 2010 and 2014.

		Phases				
	Year	Sowing	Shooting	Heading	Yellow ripening	Harvest
Winter wheat	2010	262 ± 2	133 ± 13	159 ± 1	204 ± 5	218 ± 16
	2011	263 ± 0	117 ± 2	148 ± 5	194 ± 6	203 ± 4
	2012	263 ± 1	117 ± 4	141 ± 0	195 ± 2	207 ± 2
	2013	258 ± 2	128 ± 4	150 ± 7	204 ± 4	216 ± 3
	2014	259 ± 0	113 ± 1	137 ± 5	191 ± 5	205 ± 1
Winter barley	2010	261 ± 0	119 ± 5	144 ± 2	180 ± 2	198 ± 2
	2011	262 ± 4	120 ± 4	131 ± 1	167 ± 3	187 ± 7
	2012	264 ± 1	115 ± 2	131 ± 1	171 ± 2	191 ± 1
	2013	248 ± 16	126 ± 5	149 ± 9	177 ± 2	199 ± 1
	2014	265 ± 0	108 ± 0	112 ± 0	167 ± 0	199 ± 0

detection applications or geometric accuracy assessment (Rounds, 1980; Möller et al., 2012; Tang et al., 2011; Möller et al., 2013).

A practical difference of the two calculated spectral separability indicators is that η^2 can potentially be used for a multi-class classification scenario, while the *Kolmogorov–Smirnov distance* can only be used to evaluate spectral differences of two different classes.

3.3. Classification and validation

The optimized indices were calculated for training and validation fields. An unsupervised *k-means* clustering with five iterations was applied to the indices and compared to the actual class memberships of the pixels. A confusion matrix was calculated that contains the number of pixels which were classified correctly and which pixels were assigned to a wrong class. The percentage of correctly classified pixels to the total number of pixels represents the overall classification accuracy *A*.

The classification accuracy corresponding to the highest separability metric value ($A([\eta^2 \vee d^{KS}]_{max})$ is compared to the maximum classification accuracy (A_{max}) to evaluate the capability of the metric to select the most significant parameter combination for a classification problem.

3.4. Implementation

The satellite data were atmospherically corrected using the *Fast line-of-sight Atmospheric Analysis of Spectral Hypercubes (FLAASH)* algorithm (Anderson et al., 2002). The remote sensing software package ENVI® 5.2 version (Exelis Visual Information Solutions Inc., Boulder, CO, USA) and its FLAASH® module were used for atmospheric correction.

The actual methodology was implemented within the statistical computing environment *R* (R Core Team, 2015). First, the satellite data sets were cropped and masked to the extent of the training sites for the respective harvesting season. In doing so, only the test fields, on which winter wheat and winter barley were harvested in 2011, were extracted from all satellite data sets acquired later than August 2010 and for the seasons 2012, 2013 and 2014 accordingly.

All combinations of the parameters described in Table 2 within Eq. (1) were calculated. The domain of the parameters c_1 and c_2 was chosen in a way that it includes the empirical values determined by Huete et al. (1999) and Jiang et al. (2008). The similarity measure η^2 was computed using the function *etasq()* which is included in the *R* package *heplots* (Fox et al., 2015).

The function *kmeans()* that was used for validation is included in *R*'s base distribution, while the functions *confusion.matrix()* and *similarity.index()* are included in the package *clv* (Nieweglowski, 2013).

4. Results

The first objective of this study was to develop a framework for the detection of the optimal band and parameter combination for the index permutation approach (Section 4.1). The actual optimization procedure is performed on a single data set, but this data set has to be selected out of time series of satellite images using comprehensible criteria, e.g., phenological aspects. The algorithm is then applied to generate multi-annual separability profiles (Section 4.2).

4.1. Mono-temporal index optimization

4.1.1. Phenological development

Winter wheat and winter barley show differences in their phenological behavior. The phenotypes of the target species are highly similar until heading, when grains and, especially for barley, awns are built. Hence, an acquisition date is probably best suited for wheat and barley separation, on which at least one of the target species already reached the phenological stage of heading.

In Germany, winter barley is usually sown in mid-September, shooting is observed in mid-April, heading in mid-May, yellow ripening in late June and harvest in mid-July. Winter wheat is sown between late September and mid-October and harvested in early August. Shooting is usually observed in late April, heading in late May or early June, and yellow ripening in the second half of July.

The phenological development of the selected field crops differs between locations, years and species. Within the study site, three phenological stations exist that observe phases for winter wheat. For winter barley also information observed on three stations were available, except for 2014, when only one station observed winter barley phases. The mean observed day as well as the variation within the site are listed in Table 3. In general, winter wheat reaches a phenological stage approximately 10–20 days after winter barley reached the same stage. The variations within the site are usually smaller than 5 days, which indicates a homogeneous plant development in the study region.

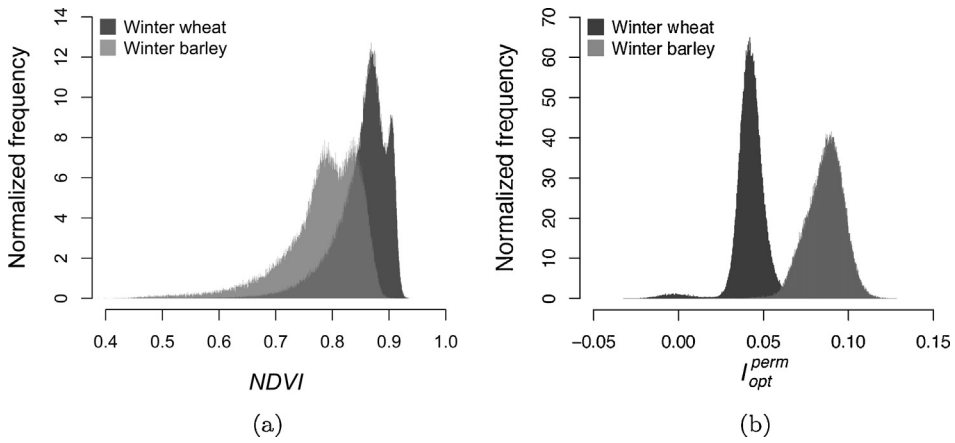

Fig. 3. Per-class index distributions of *NDVI* (a) and I_{opt}^{perm} (b) on 4th June 2014.

4.1.2. Parameter determination for formulation of the optimized index

Considering the phenological behavior of winter wheat and winter barley, the RapidEye image acquired on 4th June 2014 (*DOY* = 184) is selected to demonstrate the optimization approach derived by the index permutation, because on this date the two crops are most likely at different growth stages (Table 3) and the differences in their phenotypes (see Section 4.1.1) are expected to be visible. According to Table 3, winter barley already reached the phenological stage of heading on that date, while winter wheat did not yet.

The resulting optimal vegetation index I_{opt}^{perm} (see Eq. (1)) is characterized by $\eta^2 = 0.82$ and calculated as following:

$$I_{opt}^{perm} = \frac{R_{RE} - R_B}{R_{RE} + 7.5 \times R_B + R_{NIR} + 1} \quad (2)$$

$NDVI^{RE}$ has been found to be the best standard vegetation index I_{opt}^{s} with $\eta^2 = 0.56$. In contrast, the traditional *NDVI* only shows a η^2 value of 0.26. Finally, the comparison of I_{opt}^{perm} and *NDVI* distributions illustrates the effect of index optimization (Fig. 3). While the *NDVI* distributions of winter wheat and winter barley are characterized by a high degree of overlap, the I_{opt}^{perm} distributions are clearly distinguishable from each other.

4.1.3. Classification and validation

NDVI and I_{opt}^{perm} were calculated for all test and validation fields. A *k-means* classification was performed, and the classification

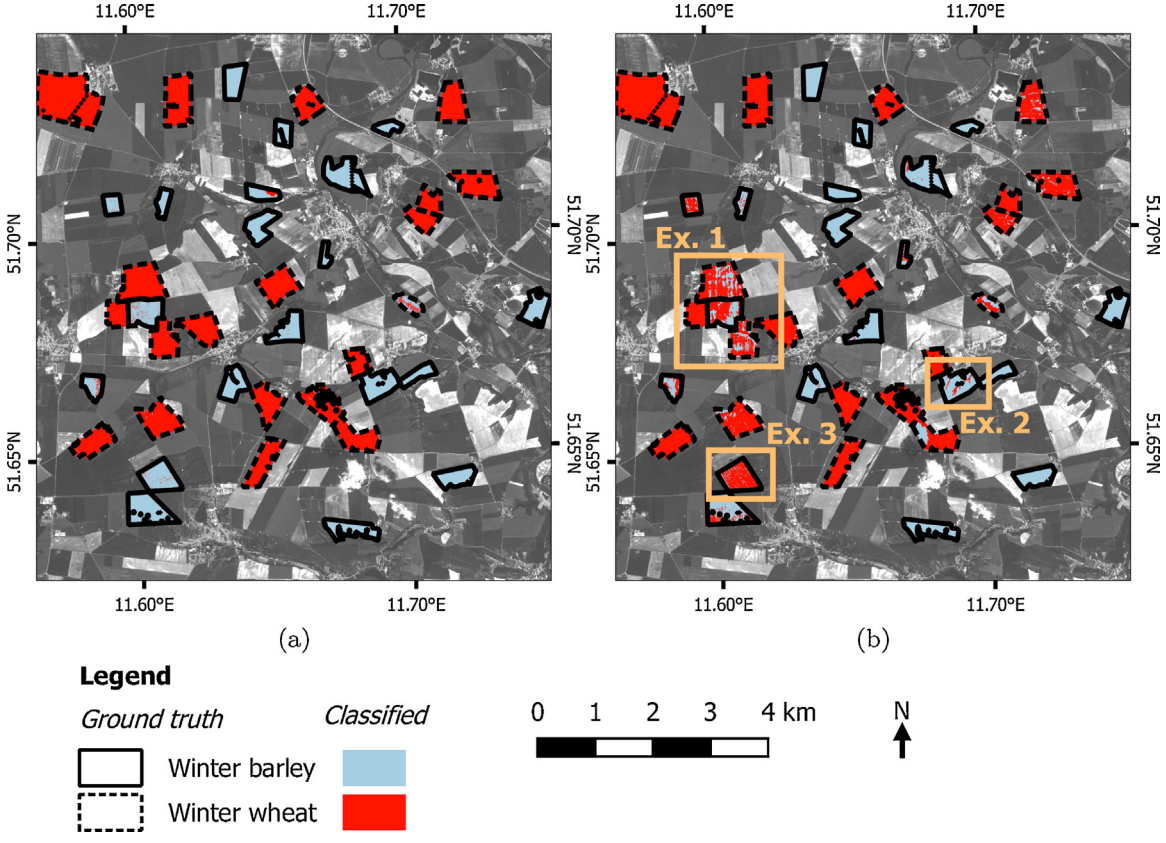

Fig. 4. *K-means* classifications based on I_{opt}^{perm} (a) and I_{opt}^{s} (b) for 4th June 2014 and actually cultivated crops. The orange boxes indicate parcels where major differences are visible (b). Projection: EPSG 4258 (Spatialreference, 2016). (For interpretation of the references to color in this figure legend, the reader is referred to the web version of this article.)

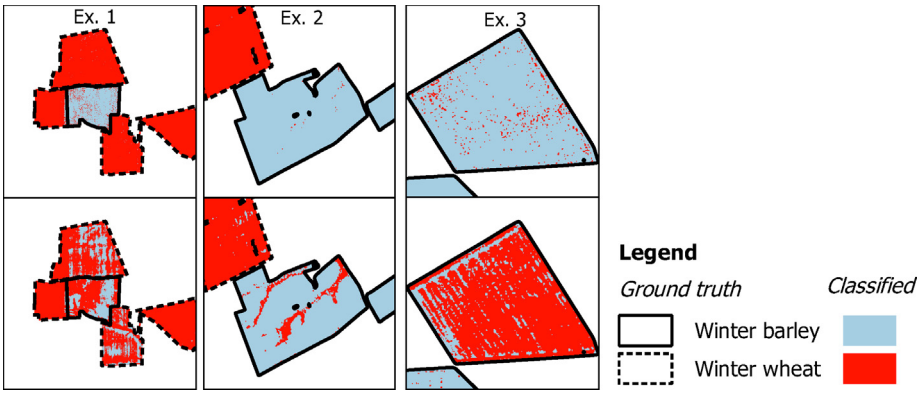

Fig. 5. Example fields for different classification results (see Fig. 4) between I_{opt}^{perm} (top row) and I_{s}^{perm} (bottom row).

accuracy was assessed (see Section 3.3). The classification results are shown in Fig. 4.

The classification based on I_{opt}^{perm} reaches an accuracy $A = 0.97$, while for I_{opt}^{s} it is only $A = 0.87$. In Fig. 5, the differences between the two index classification results are visualized on the example of three subsets (see Fig. 4):

- Example 1 shows that the classification based on I_{opt}^{perm} leads to more homogeneous parcel-specific classes. In contrast, the I_{opt}^{s} classification tends to a mixture of both crop types in one parcel (Fig. 5, left).
- In the case of example 2 (Fig. 5, center), a clearly recognizable river channel was false classified as winter wheat using $NDVI^{RE}$, while I_{opt}^{perm} is robust against phenomena associated with riverbeds such as higher soil water content, less vegetation coverage, etc. Almost the complete field was classified correctly as winter barley.
- While the classified index I_{opt}^{perm} is almost exactly corresponding to the ground truth data, some fields are nearly completely classified wrong when $NDVI^{RE}$ was used. In example 3 (Fig. 5, right), the pixels within the example winter barley field are false classified as winter wheat by about 90%.

4.2. Multi-annual separability profiles

4.2.1. Parameter determination for optimized indices

After applying the workflow on the five-year time series, a spectral separability profile has been computed which summarizes the maximal η^2 values for each acquisition date. Fig. 6 shows the results of the similarity assessment for the complete time series. The threshold of $\eta^2 > 0.26$ (see Section 3.2) is exceeded on 20 of the 43 acquisition dates. Twelve of these dates are between May and August of the respective seasons, while eight are between October and March. The summer maxima show significantly higher η^2 values. An exception is the 2012 season, when no images between mid-May and mid-August were available.

The configurations of I_{opt}^{perm} as well as I_{opt}^{s} are listed in Table 4 for all acquisition dates on which $\eta^2(I_{opt}^{perm})$ exceeds the 0.26 threshold. The three scenes acquired on 16th July 2010, 22nd July 2013 and 26th July 2014 have been excluded since the phenological observations (Table 3) indicate that barley is most likely already harvested on these dates while winter wheat is still unharvested. Visual inspections of the satellite images support these findings.

The results confirm the significance of the spectral region between red and near infrared for the detection of differences in vegetation status in general as well as for the classification of winter wheat and winter barley in particular. Consequently, the vast majority of I_{opt}^{perm} combinations include R_{NIR} (16 occurrences), followed by the R_R and R_{RE} (10 occurrences, respectively). Indices computed only of two spectral bands were selected on two dates. Only on four dates, an I_{opt}^{s} was selected that does not include the red edge band, which underlines the importance of the red edge spectral region. The bands, that were selected most frequently are R_{NIR}, R_{RE} and R_B (five occurrences) and R_{NIR}, R_{RE} and R_R with four occurrences, with different assignment to B_1, B_2 and B_3 and different scaling parameters.

The η^2 differences between I_{opt}^{perm} and I_{opt}^{s} vary throughout the time series. Especially in 2014 the optimal band combinations outperform I_{opt}^{s}, while in 2010 only small differences were observed. On three dates, I_{opt}^{s} is far below the separability threshold of 0.26 while I_{opt}^{perm} exceeds this threshold (1st May 2012, 10th and 29th March 2014). On these days, I_{opt}^{perm} includes the green band which indicates an specific importance of this spectral region for discrimination of winter wheat and winter barley that is poorly addressed by the most standard vegetation indices.

4.2.2. Classification and validation

All possible index combinations have been calculated and clustered for the training and validation fields for all of the available RapidEye images. Confusion matrices have been calculated and the overall classification accuracy was assessed. Here, A values close to 1 represent high accordance between the validation classes and the *k-means* clusters. For each element of I_{i}^{perm}, d^{KS} was also calculated.

In Table 5, the classification accuracies achieved by classification of I_{opt}^{perm} and I_{opt}^{s} as well as the classification accuracies using the index with d_{max}^{KS} are listed for the dates on which η^2 exceeds the significance threshold of 0.26.

For most of the acquisition dates, the accuracy derived by classification of the optimized index using η^2 as separability metric is higher than if other metrics or standard indices were used, except for five acquisition dates:

- On two dates (4th June 2011 and 14th November 2012), the $A(\eta_{max}^2)$ is lower than the classification accuracies of the best standard indices and the optimized index using d_{max}^{KS}. This difference is very small (1%) on 14th November 2012 but higher, 5% compared to $A(d_{max}^{KS})$ and 9% compared to I_{opt}^{s}, on 4th June 2011.
- On 29th March 2014, d_{max}^{KS} finds an index that leads to slightly (2%) higher classification accuracy than η_{max}^2.
- On 23th October 2010 and 2nd June 2011, the I_{opt}^{s} outperforms I_{opt}^{perm} by 2 and 3%.

Despite these exceptions, which are mostly characterized by only very small accuracy differences, the results underline that η^2 finds a better suited index with higher probability than d^{KS} and the optimized indices are usually better suited for the tested classification scenario than the established standard indices.

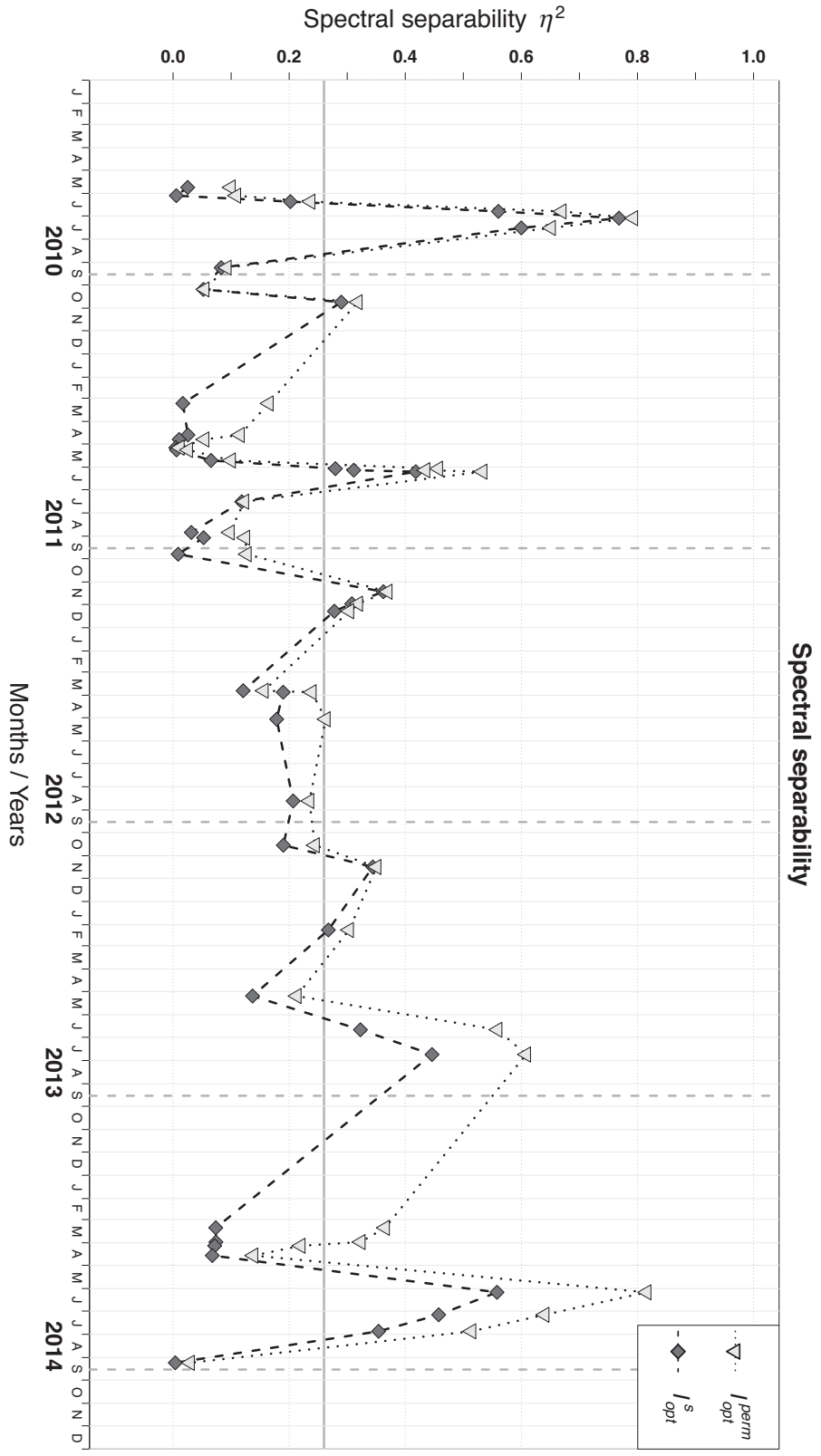

Fig. 6. Spectral separability profiles for the cropping seasons from 2010 to 2014. Points and triangles represent the acquisition dates of the RapidEye image. The bold vertical line indicates the threshold for a high association between class membership and index values, the dashed horizontal lines are the approximate sowing dates.

To underline these findings, the maximal classification accuracy of all index variants (A_{max}) was compared to the accuracy of the clustered I_{opt}^{perm} for both spectral separability measures, $A(\eta^2_{max})$ and $A(d^{KS}_{max})$, as shown in Fig. 7. A_{max} ranges between 0.974 on 3rd Jul 2010 and 0.61 on 9th September 2014. The accuracy of the clustered I_{opt}^{perm} indicated by η^2 ($A(\eta^2_{max})$), ranges from 0.974 again on 3rd July 2010 and 0.435 on 3rd June 2010. Indices determined as optimal using η^2 show a significantly higher correlation ($r = 0.90$) to the $A(d^{KS}_{max})$ values ($r = 0.77$), which illustrated the capability of η^2 for index selection for a dichotomous classification problem.

Table 4
Optimal bands and parameter values (I^{perm}_{opt}), best standard vegetation indices (I^{s}_{opt}) and corresponding $\eta^2(I^{perm}_{opt})$ and $\eta^2(I^{s}_{opt})$ values for acquisition dates of high separability.

Date	B_1	B_2	B_3	c_1	c_2	L	G	I^{s}_{opt}	$\eta^2(I^{perm}_{opt})$	$\eta^2(I^{s}_{opt})$
24 June 2010	R_{RE}	R_R	R_{NIR}	0	6	−1	1	*SRR*	0.67	0.56
3 July 2010	R_B	R_{RE}	R_{NIR}	−1	1	0	1	$NDVI^{RE}$	0.79	0.77
23 October 2010	R_R	R_{NIR}	–	−1	−1	−1	1	*SAVI*	0.32	0.29
2 June 2011	R_B	R_{NIR}	R_{RE}	1	1	1	1	EVI^{RE}	0.46	0.28
4 June 2011	R_{RE}	R_B	R_{NIR}	7.5	−1	1	1	EVI^{RE}	0.43	0.31
6 June 2011	R_R	R_{RE}	R_{NIR}	2.4	6	−1	1	EVI^{RE}	0.53	0.42
13 November 2011	R_R	R_{NIR}	–	0	−1	1	1	EVI^{RE}	0.37	0.36
29 November 2011	R_{NIR}	R_R	R_{RE}	−1	6	−1	1	*SRR*	0.32	0.31
9 December 2011	R_{NIR}	R_R	R_{RE}	−1	6	−1	1	*SRR*	0.30	0.28
1 May 2012	R_G	R_{NIR}	R_B	0	2.4	−1	1	*SRR*	0.26	0.18
14 November 2012	R_{NIR}	R_R	R_G	2.4	1	1	1	*SAVI*	0.35	0.34
6 February 2013	R_{NIR}	R_R	R_B	6	6	1	1	*WDRVI*	0.30	0.27
19 June 2013	R_{RE}	R_B	R_{NIR}	6	−1	1	1	EVI^{RE}	0.56	0.32
10 March 2014	R_G	R_B	R_R	2.4	2.4	1	1	EVI^{RE}	0.37	0.07
29 March 2014	R_G	R_{RE}	R_{NIR}	1	−1	−1	1	EVI^{RE}	0.32	0.07
4 June 2014	R_{RE}	R_B	R_{NIR}	7.5	−1	1	1	$NDVI^{RE}$	0.82	0.56
4 July 2014	R_R	R_{NIR}	R_B	2.4	7.5	−1	1	*SAVI*	0.64	0.46

Table 5
K-means classification accuracies *A* for optimized indices I^{perm}_{opt} and standard indices I^{s}_{opt} detected by using η^2_{max} and d^{KS}_{max}.

Date	I^{perm}_{opt}				I^{s}_{opt}			
	η^2_{max}	$A(\eta^2_{max})$	d^{KS}_{max}	$A(d^{KS}_{max})$	η^2_{max}	$A(\eta^2_{max})$	d^{KS}_{max}	$A(d^{KS}_{max})$
24 June 2010	0.67	0.94	0.87	0.93	0.56	0.92	0.85	0.93
3 July 2010	0.79	0.97	0.95	0.89	0.77	0.96	0.94	0.96
23 October 2010	0.32	0.72	0.62	0.72	0.29	0.75	0.55	0.75
2 June 2011	0.46	0.70	0.67	0.70	0.28	0.72	0.51	0.72
4 June 2011	0.43	0.66	0.65	0.71	0.31	0.74	0.55	0.74
6 June 2011	0.53	0.88	0.75	0.67	0.42	0.73	0.64	0.73
13 November 2011	0.37	0.83	0.57	0.70	0.36	0.82	0.50	0.79
29 November 2011	0.32	0.82	0.60	0.70	0.31	0.80	0.48	0.80
9 December 2011	0.30	0.81	0.59	0.71	0.28	0.78	0.50	0.80
1 May 2012	0.26	0.79	0.59	0.72	0.18	0.71	0.49	0.42
14 November 2012	0.35	0.85	0.57	0.86	0.34	0.86	0.57	0.86
6 February 2013	0.30	0.83	0.51	0.67	0.27	0.81	0.47	0.82
19 June 2013	0.56	0.90	0.80	0.89	0.32	0.86	0.77	0.86
10 March 2014	0.37	0.84	0.69	0.61	0.07	0.59	0.28	0.59
29 March 2014	0.32	0.73	0.54	0.75	0.07	0.58	0.23	0.43
4 June 2014	0.82	0.97	0.97	0.97	0.56	0.87	0.93	0.95
4 July 2014	0.64	0.87	0.81	0.77	0.46	0.74	0.80	0.69

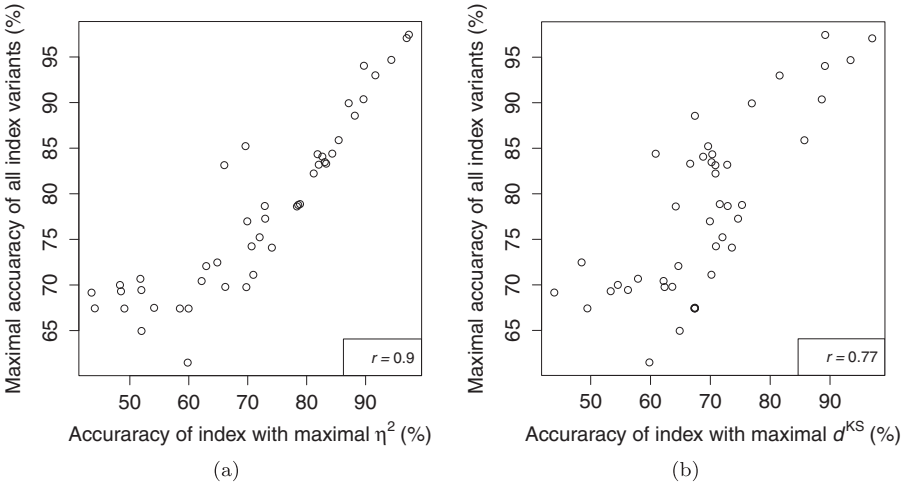

Fig. 7. Pearson's correlation coefficients and correlations between the maximum possible classification accuracy (A_{max}) and the accuracies using the I^{perm}_{opt} determined by η^2 ($A(\eta^2_{max})$, sub-figure a) and *Kolmogorov–Smirnov distance* ($A(d^{KS}_{max})$, sub-figure b).

5. Discussion

5.1. Index permutation

In principle, the presented spectral optimization procedure aims at the automatic selection of a spectral index. In doing so, we calculate numerous index variants of a *EVI*-based formulation. This includes 2-band normalized difference indices but also more complex formulations including three bands and empirical parameters that are reported to be effective in land cover classification (Henebry et al., 2004; Viña et al., 2004). This is in contrast to the approach by Rivera et al. (2014) which enables the analysis of much more complex indices computed of up to 10 bands, but does not allow the integration of empirical weighting parameters. For the crop classifications based on multi-spectral imagery, we consider indices of higher complexity as inappropriate due to two practical reasons:

1 The majority of multi-spectral satellite sensors only have less than 10 bands, and those that have more, like Sentinel-2, contain spectral bands that are not meaningful for vegetation analysis (e.g., bands for coastal applications, aerosol, cirrus and water vapour retrieval).
2 For the index optimization for classification purposes, much larger sample sizes are required to balance intra-class variations due to growth status, soil properties, fractional vegetation cover and others. In our case, we analyzed approximately 500,000 pixels/samples per data set compared to 108 ground measurements used by Rivera et al. (2014). This leads to much higher computational requirements.

5.2. Index optimization for a selected satellite image

The index optimization applied on the data set acquired on 4th June 2014 improved the classification accuracies compared to $NDVI^{RE}$. As expected, the formulation of the optimized index is based on the red edge reflectance. The optimized index is calculated using the same bands as the also tested EVI^{RE} (see Table 1). However, the weighting parameter configuration is different, and the $NDVI^{RE}$ was determined as best-suited standard index. Within the optimized index, the blue reflectance is highly accentuated by the weighting factor $c_1 = 7.5$, and the near infrared reflectance is suppressed compared to EVI^{RE}. This indicates significant differences in the blue band between barley and wheat that are most likely determined by grain and awn formation of barley as well as by chlorophyll degradation during ripening (see Section 4.1).

For the presented data set and test field selection, the optimization results in an index which is robust against within-field reflectance differences due to variations e.g., in soil water content and exposition. However, it has to be investigated in which extent the optimized index is fitted to the test data or whether classifications of larger areas can also be improved using the same number of test fields. If so, only a small number of test fields would be required to optimize the index and classify for example the complete RapidEye tile or a composite of neighboring tiles.

5.3. Multi-annual separability profiles

5.3.1. Time frame detection

Although the minor separability maximum between November and December was detected in all five years, this time frame is more uncertain than the summer peak of separability. This is mainly due to the low sun angles during this time and potentially due to anthropogenic influences like the timing of tilling and sowing.

It is worth mentioning, that the blue band was included within the optimal band combination of nine acquisition dates (see Table 4), mostly in early summer. As ripening of barley proceeded further during that time than ripening of wheat, chlorophyll decomposition as consequence of ripening also proceeded. Consequently, chlorophyll absorption in the blue spectral region is lower for winter barley than for winter wheat which makes the blue band significant for the index optimization. However, atmospheric scattering is most relevant in the blue parts of the electromagnetic spectrum. For RapidEye data of farmland in the US, Moufid (2014) found that signal-to-noise ratio for the blue band is significantly lower than for the other spectral bands. Similar to Green et al. (1988) and Dwivedi and Rao (1992), we have tested the replacement of the blue band with other bands. To estimate the loss of information by replacing the blue band with others, inter-band correlations were computed. Pearson's correlation coefficients within the test fields computed for the data set from 4th June 2014 are 0.69 and 0.78 for R_B vs. R_G and R_B vs. R_R, respectively. Consequently, clustering of the indices with band replacement leads to lowered accuracies of 0.85 and 0.82 for green and red, respectively, while the accuracy for the clustered I_{opt}^{perm} is 0.97. Taking these results into account, a replacement appears to be not appropriate.

5.3.2. Influence of varying phenological development

Since differences in the timing of spring phenological phases influence the plant's reflectance profile (e.g., Förster et al., 2012; Boschetti et al., 2009; Duveiller et al., 2012; White et al., 2009), phenological variations are probably accounting for the inter-annual shifts in the timing of the summer separability peaks. The optimization for each data set instead of a single vegetation index allows the usage of an index that is sensitive to specific reflectance characteristics of crops during a specific growth stage. This becomes obvious by comparison of years with almost identical acquisition dates available, which is the case for 2010 (6th June and 3rd July) and 2014 (4th June and 4th July).

In 2010, the July image provides the maximal η^2, while in 2014 this is the case with the image acquired in June. This shift is also visible within the phenological observations data set (see Table 3). In 2014, beginning of heading of winter barley was observed 32 days earlier than in 2010 (23rd April vs. 25th May). For winter wheat, this difference is approximately 22 days. Yellow ripening was observed approximately 13 days earlier for both crops.

So the phase combinations are different between the years on the acquisition date in June. On 6th June 2010, winter wheat did not reach the stage of heading while for winter barley heading was observed before the image acquisition. During the heading of barley, long awns are built which lead in a brighter appearance that is also visible in the reflectance spectrum resulting most likely to the separability maximum that was observed in 2010. On 4th June 2014, for both crops heading was already observed, so winter wheat also shows a more yellowish color.

Yellow ripening of winter barley was observed 17 days before the image acquisition in 2014 but only four days before the 2010 image was acquired. This indicates, that ripening proceeded much further in 2014. The proceeded ripening is effective for the reflectance spectrum since it is characterized by declining chlorophyll and water content. Simultaneously, winter wheat did not reach the stage of yellow ripening in both years on the image acquisition dates. These two findings are probably accounting for the observed higher separability in July 2014 compared to July 2010.

5.4. Classification and validation

The classification of the optimized index was demonstrated to be more accurate than for standard vegetation indices. For the acquisition date of the highest spectral separability, the optimization derives an index, which is fitted to a subset of the RapidEye tile,

while the standard indices have been designed to be applicable on up to continental scales.

The validation framework tends to indicate higher classification accuracies than applied on natural scenarios of classification. This is mainly due to the fact that within the presented dichotomous classification scenario the class number is known and no pixels exist within the image data set which do not belong to one of the target classes. In more realistic classification scenarios the possible class number is much higher or even unknown which most likely increases classification uncertainty. However, for demonstration of the algorithm the laboratory-like conditions are constructive for the comparison of the permuted vegetation indices. The transferability of the approach to natural classification schemes has to be evaluated separately.

6. Conclusions and outlook

In this study we presented a vegetation index optimization methodology to find the best index for a dichotomous classification scenario. The index, of which the class-specific histograms of two crop types are as non-similar as possible, is detected out of a huge number of systematically calculated vegetation indices. The η^2 metric was introduced as spectral separability measure which is non-parametric and thus better suitable in selecting the optimal spectral bands for species discrimination than other separability measures which require normal distributions.

The η^2 statistic was successfully applied for the detection of the vegetation index that allows the most accurate separation of two crop types. Mathematically, η^2 can also be used as spectral separability indicator for a n-class classification scenario, but its performance for such a scenario has to be tested in the future.

The optimization approach was successfully applied on a RapidEye image for spectral separation of winter wheat and winter barley. The values of the optimized index for the target crop types are highly species-dependent, which was demonstrated on classification results and histogram distribution of the index. We have also shown that the selected indices are more significant for discrimination of winter wheat and barley than widely used vegetation indices like *NDVI*, *EVI* and *SAVI*. The most significant spectral features are located between the red, red edge and near infrared parts of the spectrum.

Furthermore, we applied this optimization procedure in order to perform a multi-annual spectral separability analysis of winter wheat and winter barley. We detected two time frames, that lead to highest classification accuracies. These time frames are located in summer between June and July, and, with minor significance and higher uncertainty, between November and December. Consequently, a satellite image must be selected from the time series that was acquired during early summer to allow a most accurate classification. For winter cereals, a point in time on which at least one species already entered the phenological stage of heading is most promising but these findings are to be validated in future studies in areas of different climatic conditions. Further, the approach has to be tested for classification of other crop species.

Since Sentinel-2 will provide data of three red edge channels additional to the red and near infrared spectral regions, the application of the optimal index selection algorithm on Sentinel-2 time series has the capability to select sub-parts of the red edge region that are most significant for accurate discrimination of field crops.

If accurate phenological information, either spatio-temporal modeled using ground observations or derived from satellite data, is used as auxiliary variable, shifts in separability peaks can be explained exactly and typical growth stages, which allow most accurate classifications, can be determined.

Funding

This study was funded by the German Ministry of Economics and Energy and managed by the German Aerospace Center (DLR), grant no. 50 EE 1262 and 50 EE 1230.

Acknowledgments

We thank the DLR and Blackbridge, a Planet Labs Company, for the provision of data from the RapidEye Science Archive (RESA project ID: 653). We further thank the Ministry of Agriculture and Environment (MLU) of Saxony-Anhalt for provision of the reference data.

References

Anderson, G.P., Felde, G.W., Hoke, M.L., Ratkowski, A.J., Cooley, T.W., Chetwynd Jr., J.H., Gardner, J.A., Adler-Golden, S.M., Matthew, M.W., Berk, A., Bernstein, L.S., Acharya, P.K., Miller, D.P., Lewis, P.E., 2002. MODTRAN4-based atmospheric correction algorithm: FLAASH (fast line-of-sight atmospheric analysis of spectral hypercubes). In: AeroSense 2002. International Society for Optics and Photonics., pp. 65–71.

Bannari, A., Morin, D., Bonn, F., Huete, A.R., 1995. A review of vegetation indices. Remote Sens. Rev. 13 (1–2), 95–120.

Barnes, E.M., Clarke, T.R., Richards, S.E., Colaizzi, P.D., Haberland, J., Kostrzewski, M., Waller, P., Choi, C., Riley, E., Thompson, T., Lascano, R.J., Li, H., Moran, M.S., 2000. Coincident detection of crop water stress, nitrogen status and canopy density using ground based multispectral data. In: Proceedings of the 5th International Conference on Precision Agriculture, Bloomington, MN, pp. 16–19.

Boschetti, M., Stroppiana, D., Brivio, P.A., Bocchi, S., 2009. Multi-year monitoring of rice crop phenology through time series analysis of MODIS images. Int. J. Remote Sens. 30 (18), 4643–4662.

Cohen, J., 1988. Statistical Power Analysis for the Behavioral Sciences. L. Erlbaum Associates.

Deutscher Wetterdienst, 2015. Vorschriften und Betriebsunterlagen für die phänologischen Beobachter des Deutschen Wetterdienstes. Offenbach, Germany.

Dorigo, W., Zurita-Milla, R., de Wit, A., Brazile, J., Singh, R., Schaepman, M., 2007. A review on reflective remote sensing and data assimilation techniques for enhanced agroecosystem modeling. Int. J. Appl. Earth Obs. Geoinf. 9 (2), 165–193.

Duveiller, G., Baret, F., Defourny, P., 2012. Remotely sensed green area index for winter wheat crop monitoring: 10-year assessment at regional scale over a fragmented landscape. Agric. For. Meteorol. 166, 156–168.

Dwivedi, R.S., Rao, B.R.M., 1992. The selection of the best possible Landsat TM band combination for delineating salt-affected soils. Int. J. Remote Sens. 13 (11), 2051–2058.

Eitel, J.U.H., Vierling, L.A., Litvak, M.E., Long, D.S., Schulthess, U., Ager, A.A., Krofcheck, D.J., Stoscheck, L., 2011. Broadband, red-edge information from satellites improves early stress detection in a New Mexico conifer woodland. Remote Sens. Environ. 115 (12), 3640–3646.

Förster, S., Kaden, K., Förster, M., Itzerott, S., 2012. Crop type mapping using spectral–temporal profiles and phenological information. Comput. Electron. Agric. 89 (0), 30–40.

Fox, J., Friendly, M., Monette, G., 2015. heplots: Visualizing Tests in Multivariate Linear Models. R Package Version 1.0-16. http://CRAN.R-project.org/package=heplots.

Gitelson, A.A., 2004. Wide dynamic range vegetation index for remote quantification of biophysical characteristics of vegetation. J. Plant Physiol. 161 (2), 165–173.

Gitelson, A.A., Kaufman, Y.J., Merzlyak, M.N., 1996. Use of a green channel in remote sensing of global vegetation from EOS-MODIS. Remote Sens. Environ. 58 (3), 289–298.

Green, A.A., Berman, M., Switzer, P., Craig, M.D., 1988. A transformation for ordering multispectral data in terms of image quality with implications for noise removal. IEEE Trans. Geosci. Remote Sens. 26 (1), 65–74.

Guerschman, J.P., Paruelo, J.M., Bella, C.D., Giallorenzi, M.C., Pacin, F., 2003. Land cover classification in the Argentine Pampas using multi-temporal Landsat TM data. Int. J. Remote Sens. 24 (17), 3381–3402.

Henebry, G.M., Viña, A., Gitelson, A.A., 2004. The wide dynamic range vegetation index and its potential utility for gap analysis. GAP Anal. Progr. Bull. 12, 50–56.

Huete, A.R., 1988. A soil-adjusted vegetation index (SAVI). Remote Sens. Environ. 25 (3), 295–309.

Huete, A.R., Justice, C.O., Van Leeuwen, W.J.D., 1999. MODIS Vegetation Index (MOD 13). Version 3. Algorithm Theoretical Basis Document. NASA, Goddard Space Flight Center, Greenbelt, MD (accessed May 07.05.11).

Jiang, Z., Huete, A.R., Didan, K., Miura, T., 2008. Development of a two-band enhanced vegetation index without a blue band. Remote Sens. Environ. 112 (10), 3833–3845.

Kolmogorov, A.N., 1933. Sulla determinazione empirica di una legge di distribuzione. Giorn. Istit. Ital. Attuari 4, 92–99.

Le Maire, G., Francois, C., Soudani, K., Berveiller, D., Pontaillier, J., Breda, N., Genet, H., Davi, H., Dufrene, E., 2008. Calibration and validation of hyperspectral indices for the estimation of broadleaved forest leaf chlorophyll content, leaf mass per

area, leaf area index and leaf canopy biomass. Remote Sens. Environ. 112 (10), 3846–3864.
Liu, H.Q., Huete, A.R., 1995. A feedback based modification of the NDVI to minimize canopy background and atmospheric noise. IEEE Trans. Geosci. Remote Sens. 33 (2), 457–465.
Löw, F., Knöfel, P., Conrad, C., 2015. Analysis of uncertainty in multi-temporal object-based classification. ISPRS J. Photogramm. Remote Sens. 105, 91–106.
Massey, F.J., 1951. The Kolmogorov–Smirnov test for goodness of fit. J. Am. Stat. Assoc. 46 (253), 68–78.
Möller, M., Birger, J., Gidudu, A., Gläßer, C., 2013. A framework for the geometric accuracy assessment of classified objects. Int. J. Remote Sens. 34 (24), 8685–8698.
Möller, M., Müller, S., Doktor, D., Gläßer, C., 2012. Phenological structuring of multi-temporal RapidEye imagery. In: 2012 IEEE International Geoscience and Remote Sensing Symposium (IGARSS), pp. 4934–4937.
Moufid, T., 2014. SNR characterization in RapidEye satellite images (Master's thesis). Luleå University of Technology, Luleå, Sweden.
Murakami, T., Ogawa, S., Ishitsuka, N., Kumagai, K., Saito, G., 2001. Crop discrimination with multitemporal spot/HRV data in the Saga Plains, Japan. Int. J. Remote Sens. 22 (7), 1335–1348.
Nieweglowski, L., 2013. CLV: Cluster Validation Techniques. R Package Version 0.3-2.1. http://CRAN.R-project.org/package=clv.
Prishchepov, A.V., Radeloff, V.C., Dubinin, M., Alcantara, C., 2012. The effect of Landsat ETM/ETM+ image acquisition dates on the detection of agricultural land abandonment in Eastern Europe. Remote Sens. Environ. 126, 195–209.
R Core Team, 2015. R: A Language and Environment for Statistical Computing. R Foundation for Statistical Computing, Vienna, Austria http://www.R-project.org/.
Ramoelo, A., Skidmore, A.K., Cho, M.A., Schlerf, M., Mathieu, R., Heitkönig, I.M.A., 2012. Regional estimation of savanna grass nitrogen using the red-edge band of the spaceborne RapidEye sensor. Int. J. Appl. Earth Obs. Geoinf. 19, 151–162.
Richards, J., 2012. Remote Sensing Digital Image Analysis: An Introduction. Springer Berlin Heidelberg.
Rivera, J., Verrelst, J., Delegido, J., Veroustraete, F., Moreno, J., 2014. On the semi-automatic retrieval of biophysical parameters based on spectral index optimization. Remote Sens. 6 (6), 4927–4951.
Rounds, E.M., 1980. A combined nonparametric approach to feature selection and binary decision tree design. Pattern Recognit. 12 (5), 313–317.
Rouse Jr., J.W., Haas, R.H., Schell, J.A., Deering, D.W., 1974. Monitoring Vegetation Systems in the Great Plains with ERTS., pp. 309, NASA special publication.
Schuster, C., Förster, M., Kleinschmit, B., 2012. Testing the red edge channel for improving land-use classifications based on high-resolution multi-spectral satellite data. Int. J. Remote Sens. 33 (17), 5583–5599.
Simmons, A., Fellous, J.-L., Ramaswamy, V., Trenberth, K., Asrar, G., Balmaseda, M., Burrows, J.P., Ciais, P., Drinkwater, M., Friedlingstein, P., Gobron, N., Guilyardi, E., Halpern, D., Heimann, M., Johannessen, J., Levelt, P.F., Lopez-Baeza, E., Penner, J., Scholes, R., Shepherd, T., 2016. Observation and integrated earth-system science: a roadmap for 2016–2025. Adv. Space Res. 57 (10), 2037–2103.
Spatialreference, 2016. Catalogs of Spatial Reference Systems. http://spatialreference.org (accessed 22.02.16).
Swain, P.H., Davis, S.M. (Eds.), 1978. Remote Sensing: The Quantitative Approach, vol. 1. McGraw-ill, New York City, NY, USA.
Tang, Y., Zhang, L., Huang, X., 2011. Object-oriented change detection based on the Kolmogorov–Smirnov test using high-resolution multispectral imagery. Int. J. Remote Sens. 32 (20), 5719–5740.
Tyc, G., Tulip, J., Schulten, D., Krischke, M., Oxfort, M., 2005. The RapidEye mission design. Acta Astronaut. 56 (1–2), 213–219.
Vaiphasa, C., Ongsomwang, S., Vaiphasa, T., Skidmore, A.K., 2005. Tropical mangrove species discrimination using hyperspectral data: a laboratory study. Estuar. Coast. Shelf Sci. 65 (1–2), 371–379.
Van Niel, T.G., McVicar, T.R., 2004. Determining temporal windows for crop discrimination with remote sensing: a case study in south-eastern Australia. Comput. Electron. Agric. 45 (1–3), 91–108.
Viña, A., Henebry, G.M., Gitelson, A.A., 2004. Satellite monitoring of vegetation dynamics: sensitivity enhancement by the wide dynamic range vegetation index. Geophys. Res. Lett. 31 (4).
White, M.A., de Beurs, K.M., Didan, K., Inoue, D.Y., Richardson, A.D., Jensen, O.P., O'Keefe, J., Zhang, G., Nemani, R., van Leeuwen, W.J.D., Brown, J., de Wit, A., Schaepman, M., Lin, X., Dettinger, M., Bailey, A., Kimball, J., Schwartz, M.D., Baldocchi, D.D., Lee, J.T., Lauenroth, W.K., 2009. Intercomparison, interpretation, and assessment of spring phenology in North America estimated from remote sensing for 1982–2006. Glob. Change Biol. 15 (10), 2335–2359.
Wu, C., Niu, Z., Gao, S., 2012. The potential of the satellite derived green chlorophyll index for estimating midday light use efficiency in maize, coniferous forest and grassland. Ecol. Indic. 14 (1), 66–73.